# Theoretical Investigation of Gun Tube Erosion: Interactions of Carbon Monoxide and Hydrogen with the Iron (100) and (111) Surfaces.

Margaret M. Hurley
US Army Research Laboratory
HPCMO, Major Shared Research Center
Aberdeen Proving Ground, MD 21005

Gerald H. Lushington
Programming Environment and Training / CCM
Ohio Supercomputer Center
Columbus, OH 43212-1163

Betsy M. Rice, Genrich Krasko and Cary F. Chabalowski
US Army Research Laboratory
AMSRL-WM-BD
Aberdeen Proving Ground, MD 21005-5066

## ABSTRACT

Quantum mechanical calculations are performed on both bulk iron and the surfaces of iron represented by the (100) and (111) cleavage planes. The quantum mechanical methods being used in this study are the Pseudopotential Planewave (PP-PW) DFT as implemented in the CASTEP codes, and the Full Linearized Augmented PW (FLAPW) DFT method as implemented in the WIEN97 codes. In the first part of the study, the PP-PW theoretical treatment is benchmarked by reproducing experimental properties of iron such as the saturation magnetization, the effective magneton number, the unit cell parameter for BCC iron, the bulk modulus, and the minimum energy separations for the surface planes at the Fe(100) surface. The model used is that of a slab, and the resulting relaxation in the inter-planar distances is studied as a function of the number of layers in the slab and the number of planes relaxed in the energy minimization. In the second part of the paper, the interaction of CO with the Fe(100) and Fe(111) surfaces is studied by performing energy minimizations again using PP-PW, beginning with CO placed at an arbitrary distance and orientation from the surfaces. The resulting structures are in good agreement with available experimental data, and the binding energies are found to be in reasonable agreement with experiment. In the third part of this work a segment of the potential energy surface representing the interaction of $H_2$ with the Fe(111) surface is mapped using the FLAPW approach. The current results indicate the possibility of the $H_2$ molecule reacting with the iron to form iron hydride with no, or a very negligible, activation barrier. Finally, in the last part of this study, the development of a classical potential energy function is described. This "Tersoff" function has the desirable characteristic of describing bond-order among the iron atoms in the bulk. Calculated properties for BCC iron such as the unit cell length, atomic (i.e., unit cell) volume, cohesive energy, and the elastic (i.e, bulk) modulus are found to be in excellent agreement with the experiment. The cohesive energies for two other phases of iron, the FCC and HCP, are also predicted in good agreement with experiment. Ongoing and future work is also discussed.

## INTRODUCTION

Given the present realities of Armed Forces funding, it has become critical to exploit any possibilities for prolonging the safe usage of available equipment. In the particular case of artillery, it is apparent that the Army's present stock of gun barrels erode at rates higher than would be expected from simple physical models based on thermodynamics and kinetic theory [1,2]. Additionally, there is evidence that new propellants formulated to enhance performance of existing artillery increase the wear on the gun barrel, contravening the benefits of advanced performance [2]. It has been shown that the interaction of the propellant combustion products with the gun steel deposits high concentrations of carbon into the gun steel [3]. The properties of steel show significant changes as a function of the carbon concentration. Such things as melting point, thermal expansion coefficient, and response to stress and strain can be quite different for the various forms of iron carbide. As steel is exposed to the drastic physical conditions of high temperature and pressure, and reaction products resulting from the combustion of energetic materials, the carbon content of the steel will change. This causes an overall degradation in the surface of the steel, making it much more susceptible to melting, cracking and flaking, thus reducing its useful lifetime. In this study we are attempting to unravel the mechanistic details of the chemical reactions taking place during the combustion of energetic materials that lead to the infusion of carbon atoms into the virgin steel.

There is a second chemical process that degrades the steel and involves hydrogen. It is well-established [12,13,14] that hydrogen atoms (and perhaps molecules) can easily enter the bulk steel at the iron grain boundaries. The hydrogen atom occupies such a small volume that it can apparently diffuse with little to no barrier into these inter-granular regions and weaken the bonding between the grains. The effect enables entire grains of steel to flake-off from the surface of the steel, further degrading the integrity of the surface. This weakening of the iron bonds by hydrogen is referred to as hydrogen embrittlement. The goal is to prevent or drastically reduce the enhanced carburization and hydrogen embrittlement of the steel. To achieve this goal, we will use the understanding obtained in these studies concerning the chemical mechanisms responsible for the deposition and subsequent diffusion of carbon and hydrogen into the steel. This information will be used to suggest reformulation of the energetic materials that might reduce or eliminate this carburization process and hydrogen embrittlement.

Here we report results obtained from two quantum mechanical techniques commonly used to study solids. These are the PseudoPotential PlaneWave method (PP-PW)[4], and the Fully Linearized Augmented PlaneWave method (FLAPW)[5]. Both methods used Density Functional Theory formulated within the Kohn-Sham framework. In the PP-PW, the non-valence electrons are replaced with pseudopotentials (PPs), here chosen to be “ultra-soft” PPs developed by the scheme of Vanderbilt [15]. The single particle wave function is an orthonormalized planewave, or Bloch Function, representing the proper boundary conditions. In the FLAPW approach, the core electrons are approximated using the “Muffin Tin” description [5], and the interstitial electron densities are again described by planewaves.

To simplify the initial stages of this project, we’re using pure iron rather than steel as our starting model. This approximation is justified, in part, due to the low concentration of carbon in

virgin gun steel, i.e., ~0.4% by wt. We have begun our studies with CO attacking the Fe(111) and (100) surfaces using the PP-PW method. In this first stage, we are attempting to benchmark the accuracy of the theory against experimental data. In addition to bulk iron, there is experimental data available for CO adsorbed on both the (111) and (100) surfaces. This includes heats of desorption [6,7], and both indirect [8,9,11] and direct [7,8] structural information about the location and orientation of the CO on these surfaces. In addition, there is experimental data available supporting the catalytic bond breaking of CO on Fe(111) and estimates of the heat and rate of reaction for CO -> C + O [10]. This study attempts to reproduce the known experimental data, and support or refute suggested (but unverified) structures and locations for CO on these surfaces. Results will be shown for the calculated binding energies of CO on Fe, and structural changes occurring in the CO after adsorption onto Fe(111) and Fe(100).

While the quantum mechanical approach is inherently accurate, at the present time there is a fundamental limitation to the use of this approach in that modeling of processes involving atomistically "large" systems (even of a few hundred atoms) are still outside our computational capacity. As an alternative, certain aspects of physical behavior can be simulated at the atomistic level where interatomic interactions are described by empirical (or semi-empirical) potential models. The Body Centered Cubic (BCC) transition metals pose particular challenges because the use of empirical classical potential functions is well known to be of questionable validity. On the one hand, properties such as strong directional bonding and ferromagnetism make it necessary to consider the electronic degrees of freedom explicitly in describing the interatomic interactions.

Practically all current atomistic simulations of Fe are concerned with the BCC structure using variants of a many-body potential in one of two forms: the so-called "Embedded Atom Method" (EAM)[23,24] and the so-called "N-body" or Finnis-Sinclair (FS) potential [25]. A vast family of EAM - type models for Fe has been developed thus far (for references see, e.g. [26]). The most advanced models allow for directionality of interatomic bonds. The concept of representing bonds is usually addressed in on of two ways: (i) the tight-binding analysis utilizing moments of the electronic density of states (DOS) [27], and (ii) the well known in quantum chemistry concept of "bond order" [28]. In this work, we explore a third means for defining bonds, it is the Tersoff bond-order approach [29], which represents a type of classical, analytic function approach capable of being used in a computationally efficient manner for atomistic simulations of Fe.

## METHODS

A. DEFINITION OF CALCULATED PROPERTIES

The "Saturation Magnetization" , $M_0$, is the degree to which a substance can be magnetized by an external field at T = 0°K [21]. $M_0$ (for zero orbital angular momentum) is given by

$$\boldsymbol{M_0} = \left(\frac{\boldsymbol{N}}{\boldsymbol{V}}\right) \boldsymbol{g}\, m_{\boldsymbol{B}}\, \boldsymbol{S} \tag{1}$$

where

N = number of atoms in volume V
g = electronic g-factor = 2.0023
$\mu_B$ = Bohr Magneton in (erg/gauss)
S = total spin angular momentum

The "Effective Magneton Number", $\boldsymbol{n_b}$, is defined via the Saturation Magnetization as [16],

$$\boldsymbol{M_0} = \left(\frac{\boldsymbol{N}}{\boldsymbol{V}}\right) m_{\boldsymbol{B}}\, \boldsymbol{g}\, \boldsymbol{S} = \left(\frac{\boldsymbol{N}}{\boldsymbol{V}}\right) m_{\boldsymbol{B}}\, \boldsymbol{n_b} : \qquad \boldsymbol{n_b} = \boldsymbol{g}\, \boldsymbol{S} \tag{3}$$

and is reported by experiment [13] to be 2.22 BM for iron.

The "Bulk Modulus" of a solid, ***K***, is defined as the energy required to produce a given deformation in the solid [16]. It is given quantitatively as

$$\boldsymbol{K} = \boldsymbol{V_0} \left(\frac{\partial^2 \boldsymbol{E}}{\partial \boldsymbol{V}^2}\right)_{\boldsymbol{V_0}} \tag{4}$$

where

$\boldsymbol{V_0}$ = volume of the bulk unit cell at equilibrium
$\boldsymbol{E}$ = internal energy of $\boldsymbol{V_0}$ at T = 0°k**.**

***K*** has been calculated in this study by fitting the change in energy of the Fe BCC lattice as a function of finite differences in the volume. The changes in volume were produced by uniformly changing the cell vectors in steps of 0.01Å in the primitive unit cell. The resulting curve of ***E*** *vs.* ***V*** was then fit to a quartic polynomial and the second derivative taken explicitly.

## B. QUANTUM MECHANICAL METHODS

All the iron structures are derived from the BCC space group. The quantum mechanical methods being used in this study are the Pseudopotential Planewave (PP-PW) method and Fully Linearized Augmented Planewave (FLAPW) DFT methods familiar to most solid state theoreticians. It should be mentioned that both quantum mechanical approaches use scalable codes, and it was found that a reasonable balance between CPU residence time and throughput could be obtained on the ARL MSRC SGI Origin 2000 arrays by running eight processors per job. The PP-PW algorithms are those implemented in the CASTEP [4] codes. In the PP-PW approach, the non-valence electrons are replaced with pseudopotentials (PPs), here chosen to be "ultra-soft" PPs developed by the scheme of Vanderbilt [15]. The single particle wave function is an orthonormalized planewave, or Bloch Function, and represents the proper periodic boundary conditions for the crystal:

$$j_k(r) = e^{ik\cdot r} \sum_G c_G(k) e^{iG\cdot r} \quad (5)$$

with,

k = wave vector ("crystal momentum of the electron")
G = reciprocal lattice vector
$c_G(k)$ = coeffecients of a Fourier expansion.

The DFT exchange-correlation functionals are the GGA functionals developed by Perdew and Wang [17]. The k-point sampling is based upon the "Special k-point" generation scheme of Monkhorst and Pack [18].

The FLAPW calculations use the WIEN97 algorithms developed by Schwartz et al. at the Technical University of Vienna [5]. This method has been applied to the study of the hydrogen molecule interacting with the Fe(111) surface. The muffin tin radii where selected to be 0.70 Bohr for hydrogen and 1.80 Bohr for iron. The 100 k-points were generated on a special point grid which can be used in a modified tetrahedron integration scheme developed by Bloechl et al. [19]. A constant kinetic energy cutoff of 272 eV was used to select the planewave expansion.

## C. DETAILS OF PP-PW: SURFACE RELAXATIONS

All the surface relaxation calculations utilized the PP-PW method. The surfaces are formed from Fe slabs held at the optimized structure for the bulk using a vacuum region of 10 Å. The supercell dimensions are held constant. All kinetic energy cutoffs were set at 380 eV, which is larger than the recommended 340 eV cutoff described in the CASTEP codes as "precise". The supercell contained a 1x1 unit cell in the (X,Y) directions (with Z normal to the surface). Fe(100) slabs of 6 and 8 layers have been examined. For the 6 layer slab, only the top two layers were relaxed while the remaining atoms were frozen. For the 8 layer slab, two calculations were run. In the first, only two layers are relaxed, while in the second run three layers are relaxed.

## D. DETAILS OF PP-PW: CO ATTACK ON FE

The Fe(100) slab was represented by a supercell constructed from 2x2 unit cells spanning the (X,Y) directions, with four layers of iron set at the experimental structure of bulk iron. The inter-planar distance is then given as 1.4692 Å with a total slab thickness of 4.4 Å as measured by the nuclei positions. The CO was initially placed above the surface using a graphical user interface (CERIUS2 [4]) in an arbitrarily chosen orientation with the center of mass of the CO molecule placed approximately over the center of the square formed by four of the surface irons. The CO was given an initial bond length of 1.22 Å, where the gas phase equilibrium value is approximately 1.13 Å. The carbon was placed slightly nearer the surface at a distance of 1.0780 Å, and oxygen at a distance of 1.5087 Å. The initial optimization was done without allowing for spin polarization in the wave function. This optimized structure was then used as the starting structure for the spin polarized minimization.

For CO approaching the Fe(111) surface, a slab containing three layers of iron is used with a vacuum of 10 Å. The iron structure is that used in the CO on Fe(100) optimization, and for the (111) cleavage, the inter-planar spacing is structure was generated by hand using a graphical user interface. The CO was placed above the diamond formed by four surface irons such that the CO center of mass sits roughly above the iron atom in layer two which resides inside the surface diamond. The carbon lies 0.40 Å above the surface and oxygen 0.23 Å above the surface. The CO bond was oriented approximately parallel to the long axis of the diamond. As in the (100) case, the initial optimization was done without spin polarization of the wave function. The optimized structure from this non-polarized run was then used as the starting structure for the spin polarized optimization.

## E. DETAILS OF FLAPW: HYDROGEN ATTACK ON Fe(111)

The interaction energies for $H_2$ approaching the Fe(111) surface were calculated using the FLAPW approach. The Fe(111) slab was formed from a 2x2 unit cell with seven layers of iron, and the vacuum region is fixed at 7.2 Å. The iron structure is frozen at the experimental crystal lattice structure with a unit cell length of 2.904 Å consistent with a temperature of 916°C. To reduce the computational effort, use is made of the remaining symmetry for this slab by enforcing a plane of symmetry spanning the (X,Y) directions (where Z is normal to the surface) such that each of the two surfaces forming the slab are mirror images of one another. Hence, the model includes two hydrogen molecules, with one molecule attacking each surface of the slab and behaving in a symmetrically identical fashion.

Initially, $H_2$ molecule is placed above the (111) surface at a distance of 1.35 Å. It is oriented such that the H-H bond is held parallel to the iron surface with its center of mass lying on a vector drawn normal to the surface, and this vector intersects the surface at the center of the diamond formed by four neighboring iron (111) surface atoms. The potential energy surface (PES) is generated by manually moving the $H_2$ molecule toward the surface along the normal vector in a stepwise fashion. At each step the H-H bond length is both lengthened and contracted by one or more increments to give a mapping of the PES as a function of the H-H separation. Finally, when one of the H atoms lies near the sum of the muffin tin radii R(Fe+H),

the H-H dumbbell is rotated about this H atom to further probe the PES for the other H atom. This data will later be used to fit an analytical potential energy function for use in classical molecular dynamics simulations of hydrogen migration through an iron lattice.

## F. DEVELOPMENT OF THE TERSOFF POTENTIAL ENERGY FUNCTION.

At the present time there exists quite a few bond-order models for calculating the energetics of covalent crystals (for a review see [30]). Among these models, for our purposes, the so-called Tersoff potentials [29] are of prime interests. Formulated initially for Si crystals, the potentials were also used for C and Ge, and later generalized to allow for description of multi-component systems [29,31]. The Tersoff potentials explicitly take into account the directionality of bonds. For a one-component covalent crystal, the total energy is taken to be:

$$E = 1/2 \sum_{i \neq j} f_c(R_i - R_j) \left[V_{rep}(R_i - R_j) + V_{bo}(R_i, R_j)\right] \tag{6}$$

Here $f_c(|R|)$ is a cut-off function and $V_{rep}(R_i - R_j)$ is a repulsive pair-wise potential, having a simple exponential form.

We preserve the Tersoff's expression for the total energy, but the repulsion part, $V_{rep}(R_i - R_j)$ has been modified to allow for a strong repulsion at the distances which are smaller that half the nearest neighbor distance, $R_0$, in BCC lattice:

$$V_{rep}(R) = A \exp\left(-\beta_1 |R| + \beta_4 (0.5R_0/R)^{\alpha}\right), \tag{7}$$

The attractive, bond-order part of the energy is also preserved:

$$V_{bo}(R_i, R_j) = - B \exp\left(-\beta_2 |R_i - R_j|\right) b(R_i, R_j). \tag{8}$$

However, $b(R_i, R_j)$ is now

$$b(R_i, R_j) = \zeta_{ij}^{f}(1 + \gamma_1 \zeta_{ij} + \gamma_2 \zeta_{ij}^2 + \gamma_3 \zeta_{ij}^3 + \gamma_4 \zeta_{ij}^4 + \gamma_5 \zeta_{ij}^5 + \gamma_6 \zeta_{ij}^6) \tag{9}$$

where

$$\zeta_{ij} = \sum_{k \neq i,j} f_c(|R_i - R_k|) \exp\left(-\beta_3 |R_i - R_k|^{nz}\right) g(\theta_{ijk}) \tag{10}$$

and

$$g(\theta_{ijk}) = 1 + c \left\{1 - \beta / [1 + d (h^2 - \cos\theta_{ijk}^2)^2]\right\}^{(2\,\delta)} \tag{11}$$

## RESULTS

### A. PP-PW: SURFACE RELAXATIONS

Table 1 lists calculated and experimental properties for both bulk iron and the Fe(100) surface. Both the PP-PW and FLAPW predict the unit cell lattice constant to within ~1% of experiment, which translates into ~4 and 2% errors in the volume from the respective theories. The magnetic properties of iron (at T=0°K) are reflected in the "Effective Magneton Number", $\mathbf{n_b}$, in Table 1. The experimental value is reported to be [16] 2.22 BM, while PP-PW and FLAPW predict 2.29 and 2.21 BM respectively. This is excellent agreement between experiment and theory. The ability to correctly reproduce the magnetic properties of iron is crucial, since the structure of iron is strongly dependent upon its ferromagnetism. It is anticipated that interaction energies between organic compounds and the iron surface will also show a strong dependence on the spin state of the ground state iron. The theoretical predictions for the Saturation Magnetization, $\mathbf{M_0}$, are calculated from the predicted Effective Magneton Number and Lattice Volume. The errors in these quantities carry over into the prediction of the $\mathbf{M_0}$ values, as seen in Table 1.

The structure for many iron surfaces has been explored experimentally [20], and Table 1 includes the changes in the inter-planar distances, D**d**, both from experiment and from PP-PW theory. It should be pointed out that all the calculated shifts in plane spacings are done including spin polarization of the wave function starting with the optimized bulk structure at this level of theory. Initial tests using non-polarized wave functions produced an interplanar distance between the surface layer and the second layer of **d(1-2)** = 1.13 Å, to be compared with the experimental value of 1.36 Å. The lack of proper spin treatment produced an unacceptably large error of 17% between the calculated and experimental values. For a slab containing six iron layers and relaxing only the upper two layers, but now properly including spin polarization, PP-PW predicts a change of $\Delta$d(1-2) = -1.7% and $\Delta$d(2-3) = +1.8%. This is to be compared to the experimental values of –5±2% and +5±2% respectively. The theory underestimates the degree of contraction and expansion, but gets the trend correct. Only the top two layers were relaxed since the experiment could detect no change in the $\Delta$d(3-4) spacing. To study the effect of the number of iron layers on the result, another run was made using an eight layer slab and again relaxing only the top two layers. The results in Table 1 show that the addition of the extra two layers of iron in the slab have brought the changes slightly closer to the experimental values, with theory now predicting $\Delta$d(1-2) = -2.6% and $\Delta$d(2-3) = +2.4%. Finally, a calculation was run to see if theory predicts any change in the $\Delta$d(3-4) spacing. An eight layer slab was again run while relaxing the top three layers, and the results show only a small change for the $\Delta$d(3-4) spacing, –0.3%, from its equilibrium bulk value, while the $\Delta$d(2-3) = +1.9% is in slightly worse agreement with experiment and the $\Delta$d(1-2) = -2.6% remains unchanged. Therefore, theory supports the experimental finding [20] that no change in the Fe(100) $\Delta$d(3-4) spacing could be observed.

We have not yet performed analogous FLAPW calculations on the plane spacings in the Fe(100) surface. While the FLAPW is generally accepted to give more accurate results than the PP-PW as substantiated here by the bulk structure predictions, it can be significantly more

computationally demanding than the PP-PW methods. The relative computational demands between these methods have not yet been systematically explored, but this will be done in the near future.

## B. PP-PW: CO ATTACK ON FE

The interaction of CO with Fe(100) and Fe(111) has been explored experimentally [6,7,8,10], and this experimental data serves as a good substantiation for the reliability of the theory to predict chemical reactions at the surface. Table 2 presents results for CO interacting with both an Fe(100) (see Figure 1) and Fe(111) (see Figure 2), but primarily the (100). This was more heavily studied in this work due to the fact that CO is less reative on the Fe(100) surface, and hence far more structural data is available for CO bound to the surface. All CO interactions with the surfaces are done using an iron surface frozen at the experimental structure. To begin, the CO bond length was predicted for an isolated CO molecule with the PP-PW approach. Experiment reports this value to be 1.13 Å [22], and the calculated value is in good agreement at 1.14 Å. We see that the CO bondlength, R(CO), is substantially elongated once bound to the surface. For the Fe(100) surface without spin polarization, R(CO) = 1.353 Å, and with spin 1.312 Å. For the Fe(111) surface the analogous R(CO) distances are 2.659 and 2.709 Å, respectively. An important observation is that the CO has essentially dissociated on the (111) surface with no apparent barrier to bond breaking, as seen in experiments. It is to be concluded that the binding site found for the energy minimization on the (111) surface is the dissociative site discussed in the experiments. Our results show the oxygen bound essentially to Fe atoms in the surface plane, while the carbon embeds itself deep into the diamond shaped cavity, and has its shorted Fe-C distance of 1.72 Å with an Fe atom in the third plane. While this arrangement of the oxygen and carbon in the dissociative binding site has been suggested by experimentalists [10], there has been (to our knowledge) no experimental verification of this. This is the first known prediction of the actual location for these atoms in this site. Finally, for both the (100) and (111) surface, the Fe spin seems to have little effect on the structure or orientation of the CO molecule.

Concentrating now on the Fe(100) surface, it was seen experimentally that the most tightly bound CO on (100) is assigned to the $\alpha_3$ binding site. Here, CO sits essentially in the middle of the square formed by four surface atoms, and bisects two opposing sides of the square as shown in Figure 1. Furthermore, it is tilted away from a vector normal to the surface by either $\theta = 45\pm10°$[8] or $55\pm2°$ [7], with the latter value being presented as the more reliable one. Our calculated orientation of CO puts it in exact agreement with the general location whereby it bisects two sides of the square, and our tilt angle is calculated to be 55° for the case where spin polarization was ignored, and 49° for the presumably more accurate spin polarized result. If we assume that the latter theoretical value is more accurate, then our theoretical prediction lies midway between the two experimental predictions. Experiment [7] predicted two possible distances from the carbon atom to the plane of the Fe surface, either $R_2 = 0.2$ or $0.6\pm0.1$ Å [7]. Our spin polarized calculations predict a distance of 0.57 Å, in good agreement with the larger of the two experimental choices, thereby supporting the 0.6 value. The nearest Fe neighbor distance (from carbon) was seen to lie in the range $R_1 = 1.64$-$2.04$ Å by experiment, and our closest iron (which lies in the second iron plane nearly directly below the carbon atom) is predicted to be at a distance of $R_1 = 1.95$ Å for the spin polarized calculations. As can be seen,

the neglect of the spin causes the CO to lie somewhat closer to the surface, in poorer agreement with experiment.

The binding energies of CO on the Fe surfaces can also be seen in Table 2. While there is experimental data on binding energies for both the Fe(100) and (111) surfaces, the actual structure of the CO on the surface is characterized most thoroughly for the previously described $\alpha_3$ binding site. The experimental binding energy at the $\alpha_3$ site is predicted to be 26.2 kcal/mol [7]. This value was derived from a kinetic expression describing temperature controlled desorption experiments. In the expression for the rate constant of desorption a pre-exponential factor of $10^{13}$ $s^{-1}$ was assumed. Later experiments [8] refer back to these earlier results and claim that this value for the pre-exponential is too small, and should be in the range $10^{15}$ -$10^{18}$ $s^{-1}$, which would raise the value of the binding energy. Our calculated value with spin is 32.3 kcal/mol, in reasonable agreement with the experimental value, especially considering the fact that the pre-exponential used to derive the experimental value might be to small. When spin polarization is ignored, an unacceptably large error is introduced and produces a binding error of 87 kcal/mol, well outside the range on any observed binding energies for CO on Fe. For the Fe(111) surface, the spin polarized value is predicted to be 23.3 kcal/mol. This value lies below the experimental value of 48 kcal/mol [8] for the dissociative desorption of CO from the (111) surface. The current theoretical prediction is for a (111) surface containing only three layers of iron, and the calculated binding energy could change significantly with the addition of more planes to the slab. Such a dependence on more layers is quite possible considering the small inter-planar spacing of 0.83 Å for the (111) surface, as compared to 1.43 Å for the (100). All these calculations are being redone with simultaneous relaxation of the iron surfaces. But taken as a collection, the spin polarized data for the interaction of CO with Fe(100) and (111) is in surprisingly good agreement with experiment.

## C. FLAPW: HYDROGEN ATTACK ON Fe(111)

The main purpose for the stepwise mapping of the PES for $H_2$ approaching the Fe(111) is to produce data that can be used to develop a classical potential energy function to allow us to perform classical molecular dynamics simulations on hydrogen diffusion in iron and steel. This will be discussed in the next section. Table 3 lists the interaction energies of the $H_2$ molecule with the Fe(111) surface that have been accomplished to date. The energies included in this table are in units of eV, and are relative energies with zero taken at infinite separation of $H_2$ from the surface. As you move from left to right in the table, the $H_2$ molecule approaches the surface. As you move from top to bottom in the table, the H-H bond length is increasing. It can be seen that as the $H_2$ molecule approaches the surface, there is a steady elongation of the H-H bond with only a hint at a saddle point, or transition state (TS). To date, no TS has yet been seen in the breaking of the H-H bond. A more elaborate searching algorithm will need to be employed to determine if a TS does exist. The lowest energy location found so far for the two hydrogen atoms predicts a dissociated H-H bond length of 4.2 Å. At this structure, one of the hydrogens is apparently bound to two Fe atoms, one in the surface and one in plane two. The other hydrogen is apparently bound to an Fe in the surface at the other point of the diamond and a second Fe in the third plane. More mapping of the PES will be done to refine the PES to which the classical potential energy function will be fitted.

## D. TERSOFF POTENTIAL

Table 4 presents the results of the parameter optimization. One can see from Table 1 that the new potential reproduces the elastic (i.e., "bulk") moduli, ***K***, for the BCC phase within 4%, indicating a very good reproduction of the interatomic forces around the energy minimum. It is well known that $C_{44}$ is especially sensitive to directional bonding and is not reproduced well by the traditional EAM. One can also see that the energies of FCC and HCP are discriminated very well. The cell parameter, **a**, and atomic vulume, $W_0$, for the BCC agree to within the five significant digits of the experimentally reported values. The cohesive energies for both the BCC and FCC phases, $\mathbf{E_{coh}}$, agree with experiment to within a fraction of a percent.

Fitting the energies of Face Centered Cubic (FCC) and HCP phases of Fe was a part of the procedure of the potential calibration. The HCP experimental energy [34] was estimated from the enthalpy at the point of BCC-HCP phase transformation under pressure at 130Kbar. In this model, the phase transformation occurs at P=115Kbar. This should be considered as a reasonable agreement with experiment. This Tersoff iron potential is currently being augmented with terms to include the interaction between iron and hydrogen. Upon completion of this potential energy expression, classical molecular dynamics simulations will be performed to model the diffusion of hydrogen into and through the iron bulk. This will enable us to predict diffusion rates and preferred locations for hydrogen aggregation with ensuing changes in the iron structure.

## SUMMARY

Much progress has been made in characterizing quantum mechanical methods and classical potential energy functions for use in unraveling the chemistry responsible responsible for gun tube erosion. The quantum mechanical (QM) results have shown a good level of accuracy in predicting bulk and surface properties of Fe(100) and (111) surfaces. This includes structural and magnetic properties. The QM methods have also shown quantitative accuracy in predicting structural information for CO on Fe(100). While further improvements in the model system must be made, it appears that the QM methods are also capable of quantitative predictions for the energetics of CO interactions with the iron surfaces. This will be very useful for direct predictions of structural and mechanistic data concerning the chemistry responsible for the deposition of carbon on and into the iron surfaces. This QM data will also be used to develop classical potential functions of the Tersoff form, so molecular dynamics simulations can be performed to predict diffusion rates of carbon and hydrogen through the iron, with simultaneous predictions of structural changes at or near the iron surface. To this end, QM calculations of $H_2$ interacting with Fe(111) are well underway, and a substantial part of the PES has already been mapped.

## ACKNOWLEDGEMENTS

The authors are grateful to the HPC Modernization Office for the Challenge Award #0147 and the accompanying access to the ARL MSRC resources. The authors would also like to thank the staff of the ARL MSRC for their outstanding support of this project.

## REFERENCES


1. D.S. Downs, J.A. Lannon and L.E. Harris, U.S. Army Tech. Report ARLCD-TR-80016.
2. P.J. Conroy, P. Weinacht and M.H. Nusca, Proceedings of the 8th Army Gun Tube Dynamics Symposium, Newport, RI, May 1996.
3. E.A. Brandes, Smithells Metals Reference Book (Butterworth & Co., London, 1983).
4. CASTEP, Molecular Simulations Inc., San Diego, Versions 3.8/3.9.
5. WEIN97, Blaha, P.; Schwartz, K.; Luitz, J., Vienna University of Technology, **1997**. An improved updated of the original version by Blaha, P.; Schwarz, K.; Sorantin, P.; Trickey, S.B. *Comput. Phys. Commun.* **1990**, *59*, 399.
6. Moon, D.W.; Cameron, S.; Zaera, F.; Eberhardt, W.; Carr, R.; Bernasek, S.L.; Gland, J.L.; Dwyer, D.J. *Surface Sci.* **1987**, *180*, L123.
7. Saiki, R.S.; Herman, G.S.; Yamada, M.; Osterwalder, J.; Fadley, C.S. *Phys. Rev. Lett*. **1989**, *63*, 283.
8. Moon, D.W.; Dwyer, D.J.; Bernasek, S.L. *Surface Sci.* **1985**, *163*, 215.
9. Ganzmann, I.; Kiessling, W.; Borgmann, D.; Wedler, G. *Surface Sci.* **1992**, *269/270*, 347.
10. Whitman, L.J.; Richter, L.J.; Gurney, B.A.; Villarrubia, J.S.; Ho, W. *J. Chem. Phys.* **1989**, *90*, 2050.
11. Jiang, P.; Zappone, M., Bernasek, S.L. *J. Chem. Phys.* **1993**, *99*, 8120.
12. C.J. McMahon Jr., C.J.; in *Innovations in Ultrahigh-strength Steel Technmology*, Olson, G.B.; Azrin, M.; Wright, E.S. Eds. (*Proceedings of the 34th Sgamore Army Materials Research Conference*, Government Printing Office, Washington, DC, 1990), p. 597.
13. Kiuchi, K.; McLellan, R.B. *Acta Metall*. **1983,** *31*, 961.
14. Krasko, G.L.; Olson, G.B. *Solid State Commun.* **1991**, *79*, 113.
15. Vanderbilt, D. *Phys. Rev. B* **1990**, *41*, 7892.
16. Kittel, C. *Introduction to Solid State Physics*, John Wiley and Sons, Inc., New York, **1971**.
17. Perdew, J.P.; Chervary, J.A.; Vosko, S.H.; Jackson, K.A.; Pederson, M.R.; Singh, D.J.; Fiolhais, *C. Phys. Rev*. **1992**, *B46*, 6671 (and references therein).
18. Monkhorst, H.J.; Pack, J.D. *Phys. Rev*. **1976**, *B13*, 5188. MacDonald, A.H. 1978, B18, 5897.
19. Bloechl, P.; Jepsen, O.; Anderson, O.K. *Phys. Rev. B* **1994**, *49*, 16223.
20. Harrison, R.J.; Saeper, F.; Voter, A.F.;, Chen, S.P. Innovations of Ultra-High Strength Steel Technology, Olson, G.B.; Azrin, M.; Wright, E.S. Eds. (*Proceedings of the 34th Sgamore Army Materials Research Conference*, Government Printing Office, Washington, DC, 1990), p. 651.
21. Ashcroft, N.W.; Mermin, N.D. *Solid State Physics*, Harcourt Brace College Publishers, New York, **1976**.
22. Herzberg, G., *Molecular Spectra and Molecular Structure. I. Spectra of Diatomic Molecules*, **1950,** p. 521.
23. Baskes, M.I.; Daw, M.S.; Dodson, B.; Foils, S.M. *MRS Bulletin* **1988** vol. XIII, 28.
24. Daw, M.S.; Baskes, M.I. *Phys. Rev B* **1984,** *29*, 6443; Foils, S.M.; Baskes, M.I.; Daw, M.S. *Phys. Rev. B* **1986,** *33*, 7983; Daw, M.S. *Phys. Rev. B* **1989**, *39*, 7441.
25. Finnis, M.W.; Sinclair, J.E. *Phil. Mag*. **1984,** *A50*, 45; errata , *ibid* **1986**, ***A53***, 161.
26. Simonelly, G.; Pasianot, R.; Savino, E.J. *Phys. Stat. Sol*. **1995**, *(b) 191*,249.
27. Carlsson, A.E. in *Solid State Physics*, vol. **43** (ed. by H. Ehrenreich and D. Turnbull), p.1; A. E. Carlsson, *Phys. Rev. B* **1991,** *44*, 6590.

28. Horsfield, A.P.; Bratkovsky, A.M.; Fern, M.; Pettifor, D.G.; Aoki, M. *Phys. Rev. B* **1996,** *53*,12694; Horsfield, A. *Phil. Mag. B* **1996**, *73*, 85; Aoki, M.; Horsfield, A.; Pettifor, D.G. *J. Phase Equilibria* **1997**, *18*, 614.
29. Tersoff, J.;Phys. *Rev. Lett*. **1988**, *61*, 2879; *Phys. Rev*. **1988**, *B37*, 6991; **1988**, *B38*, 9902; *Phys. Rev*. **1989**, *B39*, 5566.
30. Balamante, H.; Halicioglu, T.; Tiller, W.A. *Phys. Rev. B* **1992,** *46*, 2250.
31. Tang, M.; Yip, S. *Phys Rev. Lett*. **1995**, *75*, 2748; *Phys. Rev.* **1995**, *B52*, 15150.
32. Wu, R.; Freeman, A.J. *Phys. Rev. B* **1993**, *47*, 3904; *B* **1993**, *47*, 6855.
33. Bendick, W.; Pepperhoff, W. *Acta Met.* **1982**, *30*, 679.
34. Giles, P.M.; Longenbach, M.H.; Marder, A.R. *J. Appl. Phys.* **1971**, *42*, 4290.

Table 1. Comparison of calculated with experimental bulk properties of BCC iron for Spin Polarized Wave Functions.

| **PROPERTY** | **EXPERIMENT** | **THEORY** | |
|---|---|---|---|
| Lattice Constant | 2.866 Å[b] | (PP-PW) | 2.825 (1.4%) |
| | | (FLAPW) | 2.850 (0.6%) |
| Lattice Volume | 23.551 Å$^3$ | (PP-PW) | 22.548 (4.3%) |
| | | (FLAPW) | 23.156 (1.7%) |
| Bulk Modulus, *K* | 170 Gpa | (PP-PW) | |
| | | (FLAPW) | 172 (1.2%) |
| Eff. Magneton Num., $n_b$ | 2.22 BM[c] | (PP-PW) | 2.29 (3.2%) |
| | | (FLAPW) | 2.21 (0.5%) |
| Sat. Magnetization, $M_0$ | 1750 cgs[c] | (PP-PW) | 1881 (7.5%) |
| | | (FLAPW) | 1772 (1.2%) |
| (100) Interplanar Spacing[b] | | 6 Layers/Opt=2[d] | |
| Δd(1-2) | −5 ± 2%[b] | −1.7% | |
| Δd(2-3) | +5 ± 2% | +1.8% | |
| | | 8 Layers/Opt=2 | |
| Δd(1-2) | | −2.6% | |
| Δd(2-3) | | +2.4% | |
| | | 8 Layers/Opt=3 | |
| Δd(1-2) | | −2.6% | |
| Δd(2-3) | | +1.9% | |
| Δd(3-4) | | −0.3% | |

a. PP-PW = Pseudopotential Planewave method; FLAPW = Fully Linearized Augmented Planewave method.
b. Change from bulk plane spacing. Bulk spacing is 2.866 Å. Ref. 20.
c. Ref. 16.
d. Label refers to the number of iron layers included in the slab/number of relaxed surface layers. Percent changes are from the optimized bulk structure at this level of theory.

Table 2. Calculated and experimental values for carbon monoxide molecule on the iron (100) and (111) surfaces.

| | EXPERIMENT | | THEORY | |
|---|---|---|---|---|
| | | | **No Spin** | **With Spin** |
| **Bond Length of CO** | | | | |
| R(Gas Phase) = 1.128 Å | | | 1.144 Å | N/A |
| R(On 100) | Elongated by at least 0.07 Å [6] | | 1.353 Å | 1.312 Å |
| R(On 111) | No Available Data | | 2.659 Å | 2.709 Å |
| **q [angle of C-O bond with normal to (100) surface]** | | | | |
| 45 ± 10°[6] and 55 ± 2°[7] | | | 55° | 49° |
| **$R_2$ [distance of carbon from (100) surface, Å]** | | | | |
| Either 0.2 or 0.6 ± 0.1[7] | | | 0.50 | 0.57 |
| **$R_1$ [carbon to nearest Fe(100) neighbor, Å]** | | | | |
| $R_1$ = 1.64 – 2.04[7] | | | 1.86 | 1.95 |
| **Binding Energy (DE in Kcal/mol)** | | | | |
| Fe(100) | $\alpha_1$ = 12.8[7] | | | |
| | $\alpha_2$ = 18.0 | | | |
| | $\alpha_3$ = 26.2* | | 86.9 | 32.3 |
| Fe(111) | $\alpha_0$ (on top) | = ?? | | |
| | $\alpha_1$ (deep-hallow) | = ?? | | |
| | | | 90.0 | 23.3 |
| | $\alpha_2$ (shallow-hallow) | = 32[8] | | |
| | $\beta$ (dissoc. desorp.) | = 48[8] | | |

* Later experiments [8] claim this value is too low due to use of a pre-exponential factor of $10^{13}$ $s^{-1}$, while recommended value value is in the range $10^{15}$ - $10^{18}$ $s^{-1}$.

**Table 3. Interaction Energy (eV) for $H_2$ Approaching a Fe(111) Surface. Calculated Using FLAPW.**

| H-H Distance (Å) | Distance of H-H Center of Mass From Surface (Å) | | | | | |
|---|---|---|---|---|---|---|
| | **1.35** | **1.20** | **1.05** | **0.90** | **0.73** | **0.65** |
| 0.7540 | -0.0250 | -0.0270 | 0.0820 | 0.2628 | 0.4720 | 0.6480 |
| 1.0670 | 0.4760 | | -0.0480 | 0.0810 | -0.3160 | -0.2620 |
| 1.4230 | 1.8460 | -0.0170 | 0.7140 | | | |
| 1.7780 | | 1.4180 | 0.5520 | -0.0250 | -0.6240 | -0.5930 |
| 2.3720 | | 1.5540 | 0.3190 | -0.3220 | -0.8140 | -0.7270 |
| 2.9880 | | | | -0.5840 | -1.2630 | -1.1940 |
| 3.5570 | | | | -1.3390 | -1.6030 | -1.8530 |
| 4.1260 | | | | -1.6330 | -2.0410 | -1.8740 |
| 4.5580 | | | | -1.9050 | -1.9480 | -1.8630 |

Table 4. Experimental and Fitted Properties of Fe (energies in V, distances in Å, atomic volumes in $Å^3$, elastic moduli in $10^2$ GPA, surface energy in ev/surface atom):

| **Description** | | Exp. Value | Calc. Value | |
|---|---|---|---|---|
| **Phase- BCC** | | | | |
| Cell Length | a | 2.8589 | 2.8589 | |
| Atomic Volume | $\Omega_0$ | 11.6833 | 11.6833 | |
| Cohesive Energy | $E_{coh}$ | - 4.28 | - 4.28 | ($E_{rep}$ =2.11521 $E_{bo}$ =-6.3952) |
| Elastic Modulus | C11 | 2.4310 | 2.3675 | |
| | C12 | 1.3810 | 1.3191 | |
| | C44 | 1.2190 | 1.2190 | |
| | C' | 0.5250 | 0.5242 | |
| | K | 1.7310 | 1.6686 | |
| Surface Energy | $E_{surf(111)}$[a] | 2.5 | 2.2439 | |
| Phase- FCC ($\Omega_0$ =11.152 )[b] | | | | |
| Cohesive Energy | $E_{coh}$ | - 4.223 | - 4.2229 | ($E_{rep}$ =2.4019 $E_{bo}$ =-6.6249) |
| Phase- HCP ($\Omega_0$ =10.398)[c] | | | | |
| Cohesive Energy | $E_{coh}$ | - 4.213 | - 4.2134 | ($E_{rep}$ =2.9406 $E_{bo}$ =-7.1540) |

a. Estimated based on *ab-initio* calculations [32]
b. The atomic volume and energies as found from experiments on high-temperature BCC-FCC polymorphic transformation [33].
c. The atomic volume and energy at the point of BCC-HCP phase transformation (130Kbar) [34]

Figure 1. Optimized geometry for carbon monoxide on the iron (100) surface as determined from PP-PW calculations including spin polarization.

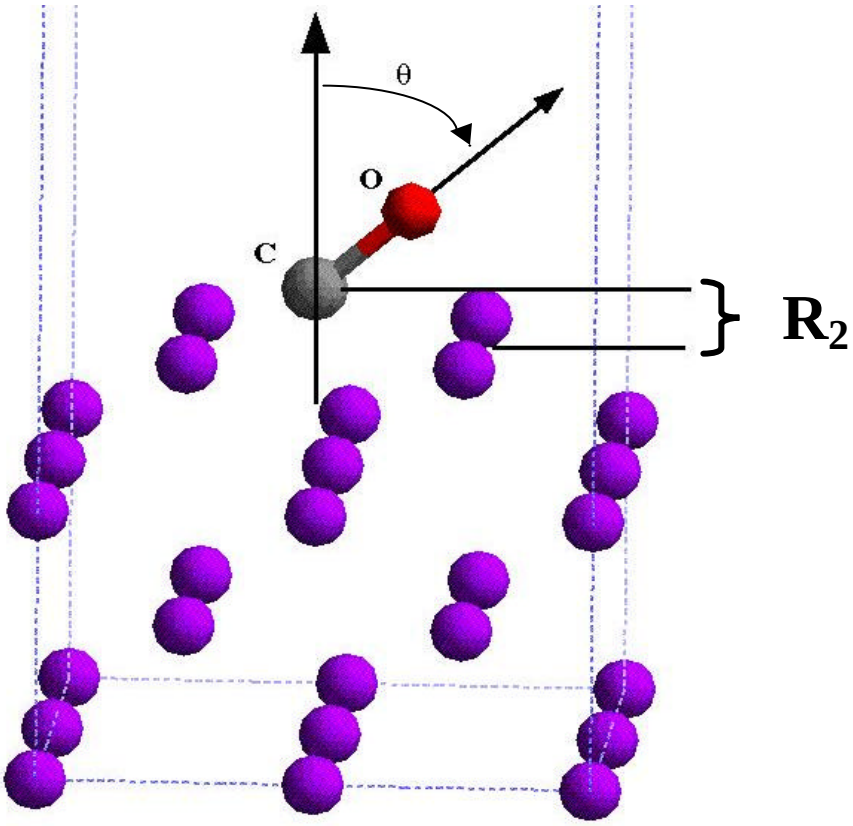

Figure 2. Orientation of the CO on the Fe(111) surface (three-layer slab) from a PP-PW optimization calculation including spin polarization. Carbon is in grey and oxygen in red. The four surface irons have been colored light blue to distinguish them from the iron in the second and third layers. See text for details.